PCCP

Accepted Manuscript

ROYAL SOCIETY OF CHEMISTRY

www.rsc.org/pccp

Cite this: DOI: 10.1039/c0xx00000x

www.rsc.org/xxxxxx

ARTICLE TYPE

Tuning the magnetic properties of Co-ferrite nanoparticles through the 1,2-hexadecanediol concentration in the reaction mixture

Carlos Moya,[a*] María del Puerto Morales,[b] Xavier Batlle,[a] Amílcar Labarta[a]

Received (in XXX, XXX) Xth XXXXXXXXX 20XX, Accepted Xth XXXXXXXXX 20XX

DOI: 10.1039/b000000x

This work reports on the effect of the 1,2-hexadecanediol content on the structural and magnetic properties of $CoFe_2O_4$ nanoparticles synthesized by thermal decomposition of metal-organic precursors in 1-octadecene. Although pseudo-spherical particles having an average size of about 8 nm and similar stoichiometry have been observed in all studied samples, a high level of variability of the crystal quality and, in turn, of the magnetic properties has been found as a function of the amount of 1,2-hexadecanediol added to the reaction mixture. The magnetic study reveals that samples progress from glassy magnetic behavior to bulk-like, ferrimagnetic order as the crystal quality improves. The analysis of the reaction mixtures by Fourier transform infrared spectroscopy at various stages of the reaction shows the key role of the 1,2-hexadecanediol on favoring the decomposition of the metal-organic precursor, formation of an intermediate $Co^{2+}Fe^{3+}$-oleate complex and, finally, the nucleation of nanoparticles at lower temperatures.

Introduction

Currently, Co-ferrite nanoparticles (NPs) are of great interest due to their high magnetic performance, including high values of the magnetocrystalline anisotropy, saturation magnetization and the magneto-optical coefficients.[1] This makes these systems excellent candidates for several technological and biomedical applications, such as information storage media,[2] detection of biomolecules by magnetic separation,[3] cancer treatment by magnetic hyperthermia[4,5] and contrast enhancement agents in magnetic resonance imaging. [6,7] However, Co-ferrite NPs show magnetic properties with high variability depending on the preparation method, what limits the standardization of those procedures for large scale applications. Consequently, the choice of a suitable synthesis method, where one can get control of the size, shape, stoichiometry and the crystallinity of the particles, is of key importance to make progress in the fundamental understanding of the properties of nanoparticulate Co-ferrite systems as compared to those of bulk-counterparts.[8] Among the conventional synthesis methods,[9] the decomposition of organic precursors at high temperature is one of the best routes to synthesize particles with narrow size distribution, high crystal quality and an atomic metal composition very close to that of stoichiometric compounds. [10,11] In this method, 1,2-hexadecanediol is commonly added to the reaction mixture as a reducing agent.[10] However, in the past, we investigated the role of 1,2-hexadecanediol in the synthesis of iron oxides NPs[12,13] and we found that this reactant was not actually necessary to synthesize magnetite NPs with bulk-like properties in a wide range of sizes.[14-16] Aiming at clarifying the role of this reactant, we synthesized 8 nm Co-ferrite NPs from a reaction mixture containing metal acetylacetonates, oleic acid as a surfactant and 1-octadecene.[17] Although we obtained a narrow size distribution and the sample was single phase with a stoichiometry very close to that of bulk Co-ferrite, NPs showed magnetic glassy behavior associated with a highly defective crystal structure,[17] in contrast with the previous case of magnetite NPs. Within this framework, in this work we demonstrate the crucial role of 1,2-hexadecanediol content in the reaction mixture as a tuning parameter that progressively improves the crystal quality and magnetic properties of Co-ferrite NPs from highly defective crystal structures with glassy behavior to NPs exhibiting single crystalline domains with bulk-like magnetism. The reaction was studied by Fourier transform infrared (FTIR) spectroscopy at several reaction stages as the time elapsed and the results showed that the decomposition of metal acetylacetonates to form a mixed-metal oleate complex takes place at earlier times and lower temperatures as the 1,2-hexadecanediol content is increased.

Experimental Section

Sample preparation

In order to clarify the effect of 1,2-hexadecanediol content and reaction time on the structural and magnetic properties of $CoFe_2O_4$ nanoparticles,[17] four samples were synthesized using iron (III) acetylacetonate (Sigma-Aldrich, 99%), cobalt(II) acetylacetonate (Sigma-Aldrich, 97%), 1,2-hexadecanediol (Sigma-Aldrich, 90%), oleic acid (Sigma-Aldrich 90) and 1-octadecene (Sigma-Aldrich 90%). All reactants were used in the synthesis without further purification.

Samples R1a, R1b and R1c. 0.71 g of $Fe(acac)_3$ (2mmol), 0.26 g of $Co(acac)_2$ (1 mmol), 0.72 g of 1,2-hexadecanediol (2.5 mmol) and 2.59 g of oleic acid (9 mmol) were mixed in 20 mL of 1-octadecene. After heating to 200 ºC and keeping the temperature constant for 2 h, the solution was heated up to reflux temperature, cooled down to room temperature and washed several times with a mixture of hexane and acetone with a volume ratio 1:3. Finally, NPs of sample R1a were collected by centrifugation at 8000 rpm. Two additional samples, R1b and R1c, were synthesized using the same route that for R1a but being the amount of 1,2-hexadecanediol 1.435 g (5 mmol)) and 2.87 g (10 mmol)), respectively. Note that the concentration of 1,2-hexadecanediol for R1c is the standard one described in literature.[10-12]

Samples R1 and R2. These particles were synthesized following a similar procedure as that used for the former reactions but without the addition of 1,2-hexadecanediol to the reaction mixtures. Particles of 8 nm in size were obtained from 0.71 g of $Fe(acac)_3$ (2mmol), 0.26 g of $Co(acac)_2$ (1 mmol) and 2.59 g of oleic acid (9 mmol) in 20 mL of 1-octadecene. The solution was heated to 200ºC under an argon flow, vigorously stirred and kept at this temperature for 2 h. After that, the solution was heated up to reflux temperature, cooled down to room temperature immediately and washed several times with a mixture of hexane and acetone with a volume ratio 1:3. NPs of sample R1 were collected by centrifugation at 8000 rpm. Sample R2, containing particles of about 12 nm in size, was prepared exactly by the same procedure as R1 but keeping it at reflux temperature during 1 h.

Experimental techniques

Particle shape and size were determined by transmission electron microscopy (TEM) using a MT80-Hitachi microscope. To prepare the samples for TEM experiments, one drop of a dilute suspension of NPs in hexane was placed onto a carbon-coated cooper grid and dried at room temperature. The size distributions were obtained by measuring at least 2000 particles and the resultant histograms were fitted to log-normal functions (see Figure 1i for samples R1and R1a-c and Figure S1c for R2, Supporting information). The mean particle size (D_{TEM}) and standard deviation (σ) were obtained from these fits (see Table 1). In order to get insight about the crystal quality of the samples, high resolution transmission microscopy (HRTEM) was carried out by using Titan high-base and JEOL-2100 microscopes (see Figures 1e-h and Figure S1b, Supporting information).

The crystallographic structure of the particles was identified by X-ray powder diffraction (XRD) performed in a PANalytical X'Pert PRO MPD diffractometer by using Cu Kα radiation. The patterns were collected within 5 and 120º in 2θ. In all cases, the XRD spectra were indexed to an inverse spinel structure (see Figure 2). The mean size of the crystal domains (D_{XRD}) obtained from XRD spectra are given in Table 1.

The Fe and Co content in the samples were determined by inductively coupled plasma-optimal emission spectrometry (ICP-OES) by using a Perkin Elmer OPTIMA 3200RL after digesting the sample in a mixture of HCl:HNO_3; 5:25, and finally diluting them with distilled water (see Table 1).

The organic fraction of the samples was evaluated by thermogravimetric analysis (TGA). Measurements were performed in a TGA-SDTA 851e/SF/1100 (Mettler Toledo) at a heating rate of 10 ºC min^{-1} in nitrogen atmosphere from room temperature up to 800 ºC.

2 mL aliquots of the reaction mixtures collected at several times along the reactions to synthesize R1 and R1a-c were studied by means of Fourier transform infrared (FTIR) spectroscopy with a Thermo SCIENTIFIC NICOLET iZ10 in the energy range between 4000 and 400 cm^{-1} with a spectral resolution of 4 cm^{-1}.

Magnetization measurements in powder samples were performed with a Quantum Design SQUID magnetometer (see Figure 3 and Figure S2b, Supporting information). Hysteresis loops, $M(H)$, were recorded at several temperatures within 5 and 300 K under a maximum magnetic field of ± 50 kOe to study the saturation magnetization M_s, and the coercive field H_c. M_s was obtained by extrapolation of the high-field region of $M(H)$ to zero field, assuming the high-field behaviour $M(H) = M_s + \chi \cdot H$, where χ is a residual susceptibility (see Table 1). M_s values were normalized to the magnetic content by subtracting the organic fraction determined by TGA measurements. H_c was defined as $H_c = (|H_c^+| + |H_c^-|)/2$, and the shift of the hysteresis loop along the field axis as $H_s = (|H_c^+| - |H_c^-|)/2$. In order to study H_s, hysteresis loops were recorded after field cooling the sample from 250 K down to the final measuring temperature under an applied magnetic field of 10 kOe. The thermal dependence of the magnetization was studied after zero field cooling (M_{ZFC}) and field cooling (M_{FC}) the samples (see Figure 4 and S2a, Supporting information). These curves were collected using the following protocol. The sample was cooled down from 300 to 2 K in zero magnetic field. Then, a static magnetic field of 50 Oe was applied and M_{ZFC} was measured while warming up from 2 to 300 K. Once room temperature was reached, the sample was cooled down again to 2 K while 50 Oe was applied. Finally, the sample was rewarmed up to 300 K and M_{FC} was collected under the applied field of 50 Oe.

Results and discussion

Structural and magnetic properties

TEM images for samples R1and R1a-c (see Figures 1a-d) show almost spherically shaped particles with narrow size distributions centered around 8 nm ($\sigma \sim 5$) (see Figure 1i and Table 1). Particles self-assemble in a hexagonal close-packing arrangement as a consequence of both the high monodispersity of all samples and the oleic acid coating that prevents particle aggregation and keep them apart from each other a few nanometers. Consequently, the concentration of 1,2-hexadecanediol in the reaction mixture did not significantly affect

either the mean size or size distribution of the particles. Interestingly enough, when the reaction mixture without 1,2-hexadecanediol was left 1 h at the reflux temperature (sample R2), spherical NPs with D_{TEM} =12 nm and a σ = 7.4 nm were obtained (see Figure S1a,c, Supporting information) indicating that the reaction time is one of the crucial parameters determining the final size distribution of the particles, indeed.[9]

However, the 1,2-hexadecanediol content in the reaction mixture gave rise to large nanostructural modifications inside the particles that could only be revealed by HRTEM images. Despite the similar values of D_{TEM} and σ for R1 and R1a-c, a gradual improvement of the crystalline quality of the NPs was observed (see Figures 1e-h) as the 1,2-hexadecanediol content was increased. While particles in R1 and R1a showed highly defective structures, with several in-volume defects and domain boundaries between randomly oriented, smaller crystal domains that add up to form crystallite aggregates, sample R1b was almost free of crystallographic defects and NPs of R1c were all single crystal domains with high structural order up to the particle surface.

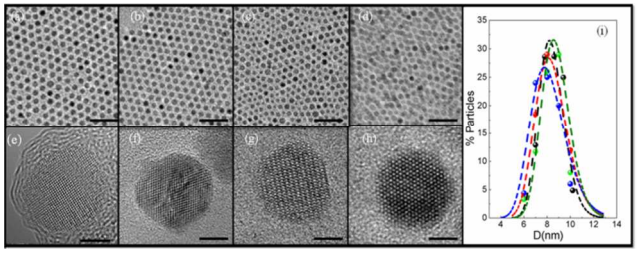

Figure 1. TEM images of the Co-ferrite NPs: (a) R1, (b) R1a, (c) R1b, (d) R1d. HRTEM images of the Co-ferrite NPs: (e) R1, (f) R1a, (g) R1b, (h) R1d. Scale bars are 40 nm in length for (a), (b), (c) and (d), and 3 nm for (e), (f), (g) and (h). (i) Particle size distributions obtained by fitting TEM histograms to a log-normal distribution function: R1 black dashed line, R1a red dashed line, R1b blue dashed line and R1c green dashed line. Experimental histograms are shown as solid spheres with the same color code.

Moreover, NPs in R2 showed also highly defective structures, as this sample was synthesized without 1,2-hexadecanediol, but with bigger crystal domains (see Figure S1b, Supporting information) because of the longer reaction time at the reflux temperature. From these results, it is unambiguously concluded that the 1,2-hexadecanediol reactant is essential to obtain single crystal particles since it somehow modifies the reaction process. It is worth noting that despite the large variation in the crystal quality of the particles, they are all single phase (core-shell structures are not observed) and their compositions, determined by ICP-OES measurements, correspond to atomic Co:Fe ratios very close to 1:2 as expected for stoichiometric Co-ferrite.

The crystal quality of the samples was also studied by XRD and the obtained diffraction patterns are shown in Figure 2. The diffraction peaks significantly sharpen when going from sample R1 to R1c as D_{XRD} increases from about one fourth of the particle diameter obtained by TEM to roughly the particle diameter (see Table 1). All XRD patterns were indexed to an inverse spinel structure without any significant trace of any other Fe and/or Co phases.

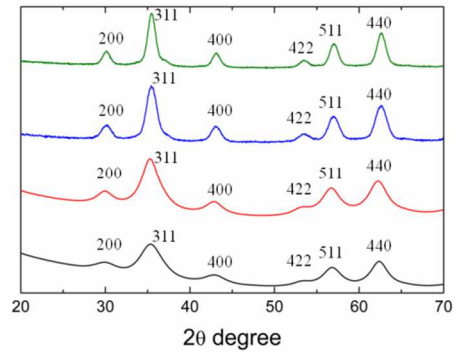

Figure 2. X-ray diffraction patterns together with the indexation of the Bragg peaks to an inverse spinel structure. Samples are as follows: R1 black solid line, R1a red solid line, R1b blue solid line and R1c green solid line.

The degradation in the crystal quality of the NPs, when the 1,2-hexadecanediol content in the reaction mixture is reduced, has dramatic consequences on their magnetic properties. The hysteresis loops at 5 K in Figure 3 range from that of R1, which resembles the one corresponding to a highly disordered and frustrated glassy-magnet, to those of samples R1b and R1c associated with an almost perfect, bulk-like ferrimagnetic ordering. On one hand, samples R1b and R1c show values of M_s and H_c (see Table 1) being similar to those published elsewhere for standard NPs of Co-ferrite.[17-22] On the other hand, NPs in R1 and R1a, containing crystal defects, domain boundaries and local anisotropies axes associated with crystal domains within the particles, show a dramatic reduction in M_s and H_c (for instance, for R1, $M_s = 25 \pm 1$ emu/g and $H_c = 6.8 \pm 0.2$ kOe) as compared to typical values of M_s and H_c for standard Co-ferrite NPs.[17-22]

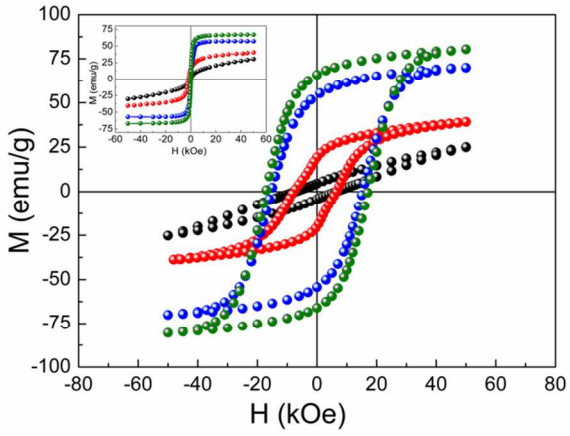

Figure 3. Hysteresis loops at 5 K. Samples are as follows: R1 black spheres, R1a red spheres, R1b blue spheres, R1c green spheres. Inset: hysteresis loops at 300 K with the same color code.

The crystalline multidomain nature of R1 and R1a NPs makes ferrimagnetic order to be arranged along the local magnetocrystalline anisotropy axes giving rise to magnetic multidomain NPs with frozen spins at the crystallite boundaries due to magnetic frustration. The existence of frozen spins in random directions and local anisotropy axes is also evident from

both the high-field linear contribution to the magnetization, which is even present at room temperature (see the main panel and the inset to Figure 3), and the high values of the closure fields of the hysteresis loops.

Sample R1a reflects an intermediate situation between the glassy behaviour of R1 and the perfect, bulk-like ferrimagnetic ordering of Co-ferrite, since crystal domains are slightly bigger in R1a than in R1. In the case of sample R2, the longer reaction time that the mixture was kept at reflux temperature promoted a further improvement in the crystallinity of the particles with respect R1, thus increasing the ferrimagnetic component of the hysteresis loops even at low temperatures (see Figure S2a and inset to Figure S2a, Supporting information).[17] However, a large shift, H_s, of the hysteresis loop along the magnetic field axis is still observable after field cooling the particles down to the measuring temperature under 10 kOe, as shown in Figure S2b in Supporting information. These horizontal shifts of the loops reveal that they are actually minor loops since the closure fields are so high due to disorder and magnetic frustration, that the reversible regime is not reached even under the maximum applied magnetic field.[12,23]

M_{ZFC} and M_{FC} curves (see Figure 4) provide further insight in the magnetic properties as the crystal quality gradually improves from sample R1 to R1c. There are significant differences between the $M_{ZFC} - M_{FC}$ curves of the four samples obtained decreasing the content of 1,2-hexadecanediol in the reaction mixture (see Figure 4). First, the peak of the M_{ZFC} curve, T_p, shifts gradually down to much lower temperatures than expected for the blocking of Co-ferrite NPs of about 8 nm in size (see Table 1 and Figure 4).[17] Second, for the most structurally defective samples (R1 and R1a), below T_p, M_{FC} is almost constant and M_{ZFC} decreases more steeply suggesting the occurrence of a freezing process around T_p due to magnetic frustration among the crystallites that form the particles rather than a simple blocking of the particle magnetizations as the sample is cooled down from the superparamagnetic regime.[17] In addition, the irreversibility temperature, T_{irr}, between M_{ZFC} and M_{FC} curves moves down as the glassy behavior of the NPs becomes more prevalent (see Table 1). Finally, the M_{ZFC} and M_{FC} curves for R2 (Figure S2c in Supporting information) suggest the formation of a ferrimagnetic component due to a partial improvement of the crystal quality, which is superimposed to the magnetic glassy behavior.

FTIR spectra

In order to elucidate the role of 1,2-hexadecanediol in the formation of the Co-ferrite NPs, 3 aliquots (2 mL) of the reaction mixtures collected at different stages of the reaction for R1 and R1a-c were studied by FTIR spectroscopy (see Figure 5). All spectra show two bands located at 1649 and 1749 cm^{-1}.[24-26] The first band corresponds to the stretching of the C=C group characteristic of the 1-octadecene (see in Figure S3 the spectrum of 1-octadecene, Supporting information), and the depth of the peak does not evolve with the reaction time since the solvent does not decompose. The second band at 1749 cm^{-1} is associated with the stretching mode of a free carbonyl and its appearance indicates the formation of the mixed $Co^{2+}Fe^{3+}$-oleate complex (see in Figure S3 the spectrum corresponding to the pure mixed oleate complex, Supporting information).

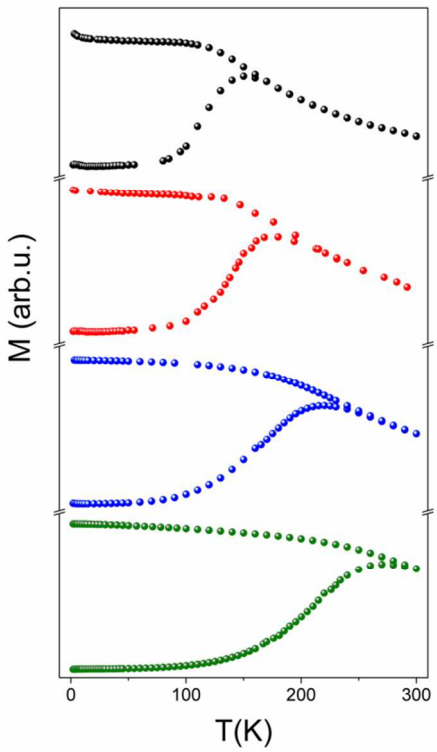

Figure 4. $M_{ZFC}-M_{FC}$ curves as a function of temperature. Samples are as follows: R1 black spheres, R1a red spheres, R1b blue spheres, R1c green spheres.

Interestingly, this band is enhanced by the increase in the 1,2-hexadecanediol content for all three studied stages of the reaction (Figures 5a-c). Moreover, some other revealing differences are observed between the spectra in Figures 5a-c. Figure 5a shows the FITR spectra of the reaction mixtures (R1-R1c) once the temperature has just been risen to 200 ºC. All the spectra in Figure 5a show the typical bands between 1574 and 1524 cm^{-1} corresponding to the stretching of the C=C and C-O groups of the metal acetylacetonates (see in Figure S3 the spectra of Fe and Co acetylacetonates, Supporting information).[27,28] It is worth noting that a drop in the depth of these peaks is observed when the concentration of 1,2-hexadecanediol in the reaction mixture is increased indicating that this reactant favors the decomposition of the metallic organic precursors. This effect is much more pronounced after 2 h at 200 ºC (see Figure 5b) where the FTIR spectra for the reaction mixtures with 1,2-hexadecanediol do not show any significant trace of acetylacetonates, while the spectrum for R1 still shows these peaks almost unaltered. Finally, Figure 5c shows the FTIR spectra of the reaction mixtures (R1-R1c) at 320 ºC. Surprisingly, the spectrum for R3 still shows the bands between 1574 and 1524 cm^{-1} indicating that the decomposition of the metal acetylacetonates has not yet fully completed.[27,28] Besides, a new band appears around 1715 cm^{-1} in the reaction mixtures R1a-c associated with the stretching mode of the C=O groups of the mixed $Co^{2+}Fe^{3+}$-oleate complex that is linked to the particle surface, [25] which is detectable at the three stages of the reaction at least for the two reaction mixtures with the highest 1,2-hexdecanediol concentration. The appearance of this peak signals the onset of the formation of the Co-ferrite NPs.

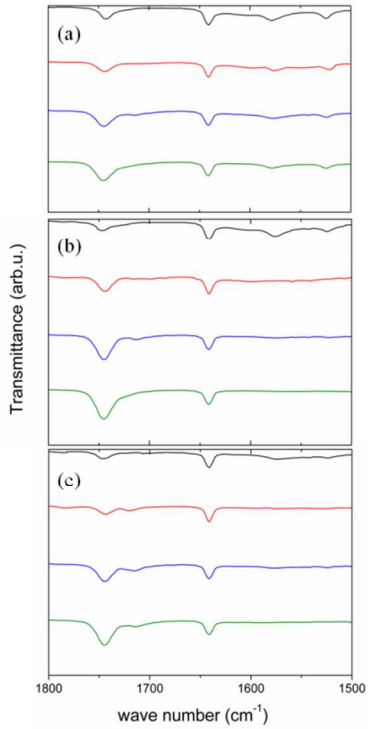

Figure 5. FTIR spectra for the reaction mixtures at (a) 200 ºC (0 min), (b) 200 ºC (120 min) and (c) 320 ºC (0 min). Curves are as follows: R1 black solid line, R1a red solid line, R1b blue solid line, R1c green solid line.

Summarizing, the analyses of the reaction mixtures by FTIR show that the 1,2-hexadecanediol content favors both the decomposition of Fe and Co acetylacetonates, and the formation of the mixed $Co^{2+}Fe^{3+}$-oleate complex, thus lowering the temperature at which the nucleation of the NPs starts. This is pretty obvious in the case of the reaction mixture for R1c (that with the standard concentration of 1,2-hexadecanediol in literature), where after 2 h at 200 ºC, there are not any traces of metal acetylacetonates and an intense band around 1749 cm^{-1} reveals that they are fully decomposed to form a mixed-metal oleate complex.[25] On the contrary, the reaction mixture for R1 after 2 h at 200 ºC clearly shows the presence of iron and cobalt acetylacetonates and only traces of the mixed-metal oleate complex. The processes that take place in the nucleation and growth of NPs may include the crystallization of small clusters, coagulation, and finally coalescence of small subunits to form the NPs and/or particle growth by diffusion.[29,30] Our results suggest that Co-ferrite NPs synthesized with a low concentration of 1,2-hexadecanediol have defective crystallographic structures due to a partial decomposition of Fe and Co acetylacetonates yielding a partial formation of the mixed-metal oleate complex, that in turn, leads to retarded nucleation and a faster growth by aggregation. In contrast, samples with higher amount of 1,2-hexadecanediol proceed through single nucleation that takes place at lower temperature and a slower particle growth by diffusion (see Figure 6b for the schematics of the process). In addition, even though the amount of 1,2-hexadecanediol slows down the particle growth leading to more ordered crystalline particles, it seems to not affect the nucleation process in terms of the number of formed nuclei since similar particle sizes and size distributions are obtained no matter the amount of this reagent. So, ions in the reaction mixture diffusing to the nanoparticle surface have more time to find the appropriate position. In fact, apart from the reducing role of the 1,2-hexadecanediol, it has been shown to serve as a template although not being as efficient as oleic acid and/or oleylamine.[31]

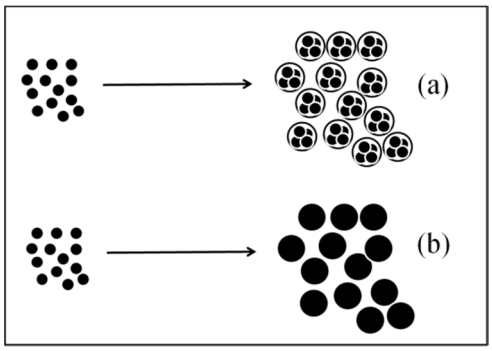

Figure 6. Schematics of the two types of particle growth observed in the samples: (a) nucleation, growth and partial coalescence of smaller subunits; (b) single nucleation and uniform growth by difusion.

Conclusions

In this work, we have demonstrated the key role of 1,2-hexadecanediol in the formation of Co-ferrite NPs with high crystal quality. The study of the reaction mixtures by FITR showed that this reactant promotes the decomposition of the metal-organic precursors, facilitating the formation of the intermediate mixed-metal complex at lower temperature. Without this reactant it is also possible to synthesize single phase, monodisperse Co-ferrite NPs of similar size and having the correct stoichiometry, but in fact being crystallite aggregates constituted of randomly oriented smaller crystal domains. The crystalline multidomain nature of the particles makes ferrimagnetic order to be arranged along the local magnetocrystalline anisotropy axes, giving rise to high magnetic frustration at the crystallite boundaries thus yielding a magnetic glassy behavior. The final crystal quality of the particles can be gradually improved by the addition of an increasing amount of 1,2-hexadecanediol to the reaction mixture and the various samples prepared reveal the close relationship between the crystal properties and magnetic behavior, since a progression from magnetic glassy behavior towards bulk-like ferrimagnetism is observed. All the foregoing could be useful to tailor the magnetic properties of Co-ferrite NPs for a specific application demanding lower/higher values of either the saturation magnetization and/or the coercive field. For instance, it may be of interest to decrease the ratio between remanent and saturation magnetizations in order to minimize particle aggregation due to dipolar interactions when they are delivered in the form of a colloidal suspension for *in vivo* applications. Besides, it might allow tuning the effective blocking temperature of the NPs from above room temperature down to about 150 K with the purpose of maximizing the absorption of an external radiofrequency excitation due to Neel relaxation to improve heat dissipation in hyperthermia applications. Moreover, it has been shown that the specific absorption rate in hyperthermia can be enhanced using some kind of multicore particles rather than single particles[32]. It is then suggested that the

crystalline multidomain nature of these Co-ferrite nanoparticles could also yield a similar heat dissipation enhancement.

All in all, the 1,2-hexadecanediol concentration in the reaction mixture can be considered as a tunable parameter that controls the final magnetic properties of monodisperse, stoichiometric Co-ferrite NPs.

Acknowledgements

This work was supported by Spanish MINECO (MAT2011-23641, MAT2012-33037, MAT2013-48054-C2), Catalan DURSI (2014SGR220) and European Union FEDER funds (Una manera de hacer Europa). C. Moya acknowledges Spanish MINECO for a Ph.D. contract (BES-2010-038075) and a three months stay at the ICMM-CSIC (Madrid).

Notes and references

[a] *Departament de Física Fonamental, Institut de Nanociència i Nanotecnologia, Universitat de Barcelona, Barcelona, Spain. E-mail: cmoya@ffn.ub.es*

[b] *Instituto de Ciencia de Materiales de Madrid, CSIC. C/Sor Juana de Inés de la Cruz 3, Campus de Cantoblanco, Madrid, Spain. E-mail: puerto@icmm.csic.es*

Electronic Supplementary Information (ESI) available: For R2: TEM and HRTEM characterization and particle size distribution. Hysteresis loops at 5 and 300 K, Hysteresis loops after field cooling the sample under 10 kOe from 250 K down to the final measuring temperature ,zero field cooling and field cooling magnetizations as a function of temperature. FTIR spectra for iron (III) acetylacetonate, cobalt (II) acetylacetonate, $Co^{2+}Fe^{3+}$-oleate complex and 1-octadecene.

1 B. D. Cullity, C. D. Graham, *Introduction to Magnetic Materials*; 2011.

2 T. Fried, G. Shemer, G. Markovich, *Advanced Materials*, 2013, **13**, 1158.

3 A. G. Pershina, A. E. Sazonov, L. M. Ogorodova, *Russian Journal of Bioorganic Chemistry*, 2009, **35**, 607.

4 E. L. Verde, G. T. Landi, J. A. Gomes, M. H. Sousa, A. F. Bakuzis, *Journal of Applied Physics*, 2012, **111**, 123902.

5 E. Mazario, N. Menéndez, P. Herrasti, M Cañete, V. Connord, J. Carrey, *The Journal of Physical Chemistry C*, 2013, **117**, 11405.

6 C. Sun, J. S. H. Lee, M. Zhang, *Advanced drug delivery reviews*, 2008, **11**, 1252.

7 C. Cannas, A. Musinu, A. Ardu, F. Orrù, D. Peddis, M. Casu, R. Sanna, F. Angius, G. Diaz, G. Piccaluga, *Chemistry of Materials*, 2010, **11**, 3353.

8 X. Batlle, A. Labarta, *Journal of Physics D: Applied Physics*, 2002, **35**, R15.

9 A. G. Roca, R. Costo, A. F. Rebolledo, S. Veintemillas-Verdaguer, P. Tartaj, T. González-Carreño, M. P. Morales, C. Serna, C. *J. Journal of Physics D: Applied Physics*. 2009, **42**, 224002.

10 S. Sun, H. Zeng, *J. Am. Chem. Soc.* 2002, **124**, 8204.

11 S. Sun, H. Zeng, D. B. Robinson, S. Raoux, P.M. Rice, S. X. Wang, G. Li, *J. Am. Chem. Soc.* 2004, **126**, 273.

12 X. Batlle, N. Pérez, P. Guardia, O. Iglesias, A. Labarta, F. Bartolomé, L. M. García, J. Bartolomé, A. G. Roca, M. P. Morales, C. J. Serna, *J. Appl. Phys*. 2012, **109**, 07B524.

13 P. Guardia, A. Labarta, X. Batlle, *The Journal of Physical Chemistry C*. 2010, **115**, 390.

14 N. Pérez, F. López-Calahorra, A. Labarta, X. Batlle, *Phys. Chem. Chem. Phys*. 2011,**13**, 19485.

15 P. Guardia, N. Pérez, A. Labarta, X. Batlle, *Langmuir*. 2010, **26**, 5843.

16 P. Guardia, J. Pérez-Juste, A. Labarta, X. Batlle, L.M. Liz-Marzán, *Chemical Communications*. 2010, **46**, 6108.

17 C. Moya, G. Salas, M.P. Morales, X. Batlle, A. Labarta, *J. Mater. Chem. C*, 2015, Accepted Manuscript. DOI: 10.1039/C4TC02889A.

18 D. Peddis, F. Orru, A. Ardu, C. Cannas, A. Musinu, G. Piccaluga, *Chem. Mater*, 2012, **24**, 1062.

19 T. E. Torres, A. G. Roca, M. P. Morales, A. Ibarra, C. Marquina, M. R. Ibarra, G. F. Goya, *Journal of Physics: Conference Series*, 2010, **200**, 072101.

20 L. I. Cabrera, Á. Somoza, J. F. Marco, C .J. Serna, M. P. Morales, *J. Nanoparticle* Res, 2012, ***14*****,** 873.

21 Q. Song, Z. J. Zhang, *J. Am. Chem. Soc*, 2004, **12**, 6164.

22 N. Bao, L. Shen, Y. Wang, P. Padhan, A. Grupta, *J. Am. Chem. Soc*, 2007, **129**, 12374.

23 J. Nogués, J. Sort, V. Langlais, V. Skumryev, S. Suriñach, J. S. Muñoz, M. D. Baró, *Physics Reports*, 2005, **422**, 65.

24 A. P. Herrera, L. Polo-Corrales, E. Chavez, J. Cabarcas-Bolivar, N. C. Oswald Uwakweh, C. Rinaldi, *JMM*, 2013, **328**, 41.

25 J. Park, A.Y. K. Hwang, J-G. Park, H-J. Noh, J-Y Kim, J-H. Park, J-H.; Hwang, N-M; Hyeon, *Nature Materials*, 2004, **3**, 891.

26 To see the FTIR spectrum of 1-Octadecene: http://webbook.nist.gov/cgi/cbook.cgi?ID=C112889&Mask=80#IR-Spec.

27 To see the FITR spectrum of $Co(acac)_2$: http://www.sigmaaldrich.com/spectra/ftir/FTIR003222.PDF.

28 To see the FITR spectrum of $Fe(acac)_3$: http://webbook.nist.gov/cgi/cbook.cgi?ID=C14024181&Mask=80.

29 P. Tartaj, M. P. Morales, S. Veintemillas-Verdaguer, T. González-Carreño, C. J. Serna, *J. Phys. D. Appl. Phys*, 2003, **36**, R182.

30 V. K. LaMer, R. H. Dinegar, *J. Am. Chem. Soc,* 1950, **72**, 4847.

31 A. C. Christopher, R. B. Andrew, *J. Mater. Chem.*, 2008, **18**, 4146.

32 P. Hugounen, M. Levy, D. Alloyeau, L. Lartigue, E. Dubois,V. Cabuil, C. Ricolleau, S. Roux,´C. Wilhelm, F. Gazeau, R. Bazzi, *J. Phys. Chem. C*, 2012, **116**, 15702.

Table 1. Summary of the structural, microstructural and magnetic parameters of the samples.[a]

Samples	D_{TEM} (nm)	σ (nm)	D_{XRD} (nm)	T_p (K)	Co:Fe (ICP-OES)	T_{irr} (K)	M_s at 5 K (emu/g)	M_s at RT (emu/g)	H_c at 5 K (kOe)	H_c at RT (kOe)
R1	8.6	5.2	2.1(0.6)	150	1.0:2.0	170	25(1)	20(1)	6.8(0.2)	SPM[b]
R1a	8.4	5.0	3.2(0.4)	180	1.0:2.0	213	38(1)	31(2)	7.3(0.3)	SPM
R1b	8.8	5.3	6.2(0.4)	222	1.0:2.0	250	70(2)	60(2)	15.1 (0.3)	SPM
R1c	8.1	4.9	8.0(0.2)	270	1.0:2.0	300	79(2)	67(1)	18.2 (0.2)	0.007(0.001)
R2	12.2	7.4	2.9 (0.4)	>300	1.0:2.0	>300	35(1)	30(1)	9.1(1)	0.066(0.001)

[a] The values in parentheses indicate the experimental error of the data

[b] Stands for superparamagnetic behaviour